Synchronization and clustering of synthetic genetic networks: A role for cis-regulatory modules

Jiajun Zhang,[1] Zhanjiang Yuan,[1] and Tianshou Zhou[1,2,*]

[1]*School of Mathematics and Computational Science, Sun Yat-Sen University, Guangzhou 510275, China*

[2]*State Key Laboratory of Biocontrol and Guangzhou Center for Bioinformatics, School of Life Science, Sun Yat-Sen University, Guangzhou 510275, China*

(Received 8 October 2008; revised manuscript received 22 February 2009; published 2 April 2009)

The effect of signal integration through cis-regulatory modules (CRMs) on synchronization and clustering of populations of two-component genetic oscillators coupled with quorum sensing is investigated in detail. We find that the CRMs play an important role in achieving synchronization and clustering. For this, we investigate six possible cis-regulatory input functions with AND, OR, ANDN, ORN, XOR, and EQU types of responses in two possible kinds of cell-to-cell communications: activator-regulated communication (i.e., the autoinducer regulates the activator) and repressor-regulated communication (i.e., the autoinducer regulates the repressor). Both theoretical analysis and numerical simulation show that different CRMs drive fundamentally different cellular patterns, such as complete synchronization, various cluster-balanced states and several cluster-nonbalanced states.

DOI: 10.1103/PhysRevE.79.041903 PACS number(s): 87.16.Yc, 05.40.−a

I. INTRODUCTION

Decoupling simple networks from their native yet often complex biological settings can lead to valuable information regarding evolutionary design principles. This motivates the design and construction of synthetic genetic networks resembling submodules of natural circuitry *in vivo,* which in turn lead to the construction of devices and software capable of performing elaborate functions in living cells [1]. Due to recent advances in bioengineering technology, several prototype synthetic genetic motifs, such as logic gates [2,3], toggle switches [4,5], and oscillators [6–8], have been successfully constructed. These simple architectures are thought of as essential modules in living organisms. Based on them, complementary approaches have been developed to explore the relationship between the structure and function of more complex genetic circuits [9,10].

A natural step in the design of artificial gene networks would be to include a mechanism of intercell coupling that would globally enhance, given that cells are frequently subject to chemical signals from neighboring cells, the oscillating response of the system. The most common communication mechanism with such a function is quorum sensing, the ability of bacteria to communicate with each other through signaling molecules that are released into the cellular environment. Quorum sensing has led to programed population control in a bacterial population [11–29]. Through such a mechanism, the ability of cells to communicate with one another allows them to coordinate the behavior of the entire community, where gene expression is regulated in response to the local cell population density [30]. A well-defined example of coordinated global behavior in bacteria is a population of genetic relaxation oscillators coupled to a quorum-sensing apparatus, which can achieve synchronization through the so-called fast threshold modulation mechanism [18]. Coupling, however, can be devised in different ways, e.g., attractive or repulsive cell-to-cell communication [18,19,23,28], in synthetic systems. Different couplings would lead to different dynamic patterns, such as synchronization, clustering, and multistability [23,28].

Why is there such a difference in cellular patterns when different types of cellular communication are employed? Actually, biological functions appearing as collective behaviors may arise from a particular module that integrates intracellular and extracellular signals. Such a module is now known as cis-regulatory module (CRM), which contains a cluster of binding sites for transcription factors (TFs) and determines the place and timing of gene action within the network. For example, the CRM in the sea urchin embryo can control not only static spatial assignment in development but also dynamic regulatory patterning [31]. TFs are often integrated in a combinatorial logic manner. Moreover such a combination may take different schemes [32–37], leading to different CRMs. In fact, from views of evolutionism, CRMs are changeable, e.g., cis-regulatory mutations [38], and such a mutation constitutes an important part of the genetic basis for adaptation. However, how different CRMs affect collective behaviors across ensembles of genetic oscillators with cell-to-cell communication remains to be fully explored.

In this paper, we investigate this question in detail and find that CRMs play a significant role in the mode of dynamic patterns at the cellular population level. For example, the CRMs can drive fundamentally different cellular patterns such as synchronization and clustering. We first design and construct a multicellular network with a CRM, using a variant of the synthetic genetic relaxation oscillator developed in *Escherichia coli* [8] and utilizing quorum sensing to communicate between cells. Since different CRMs due to cis-regulatory mutations [38] lead to different types of cis-regulatory input functions (CRIFs) such as AND, OR, ANDN, ORN, XOR, and EQU, we then investigate the effects of these different CRIFs on cellular patterns to support our conclusion. We emphasize that since the proposed genetic relaxation oscillator is composed of interacting positive and negative feedback loops, and this circuit topology is common in genetic oscillators such as cell cycle and circadian clocks

*mcszhtsh@mail.sysu.edu.cn

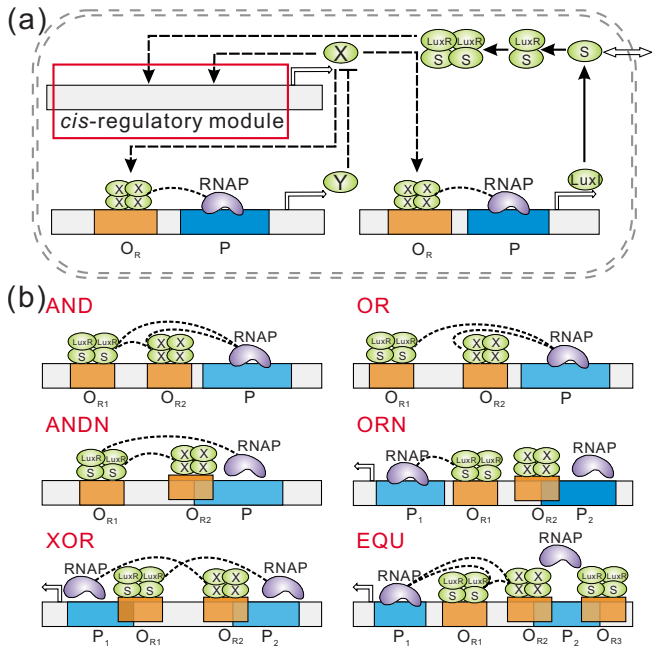

FIG. 1. (Color online) (a) Schematic diagram of the network of genetic relaxation oscillators with a cis-regulator module, where the right bidirectional arrow indicates that S can freely diffuse through the cellular membrane. (b) Six cis-regulatory constructs for implementations of six different logic functions. In (a) and (b), X, Y, and LuxI denote the proteins; P_1 and P_2 represent the promoters. O_R stands for operator site, whereas RNAP stands for RNA polymerase. We use offset and overlapping boxes to indicate the mutual repression and the dashed lines to indicate the cooperative interaction.

[39–45], our conclusion on how CRMs influence the dynamics of genetic circuits with this shared topology will be of general relevance to a wide range of cellular processes.

II. MATHEMATICAL MODEL AND THEORETICAL ANALYSIS

A. Model

First, we report our design on a network of coupled synthetic genetic relaxation oscillators with a CRM, which is schematically shown in Fig. 1. The core oscillator is a variant of the genetic relaxation oscillator proposed in Ref. [8]. In such an oscillator, the activator X (CII) and the repressor Y are under the control of different promoters from the λ phage virus. In Fig. 1(a), X is the autocatalytic portion of the oscillator, whereas Y is a protease that degrades X. Both genes x and y are activated by protein X. Such a circuitry not only is a useful architecture for understanding information processing of simple oscillators but also appears as a common core motif in biological contexts [39–44]. In our design, we utilize the quorum-sensing apparatus of the bacterium *Vibrio fischeri* [30] to communicate between cells. This cell-to-cell communication system operates by diffusing a small molecule [also called autoinducer (AI)] into the environment. Since the communication is implemented by the signal molecule which regulates the activator X, we refer to it as activator-regulated communication. When this molecule binds to a regulatory protein (LuxR), both it and X bind the regulatory region of gene x or y and combinatorially modulate the transcription rate. Many of these combinational effects are performed by a CRM, which can function as an analogous implementation of logic gates. The corresponding CRM contains a cluster of binding sites of two different TFs that control the activation or repression of a gene. These TFs may be either activators enhancing the binding or the activity of the RNA polymerase in the cognate promoters, or repressors blocking this binding, or both via the mechanism of "regulated recruitment" [46]. Based on the possible combination of the two TFs, the CRM can perform different logic functions with different implementations, as shown in Fig. 1(b). Limited by the regulatory structure of the relaxation oscillator (more precisely, the TF X serves as activator only), we have six biologically feasible CRM designs: AND, OR, ANDN, ORN, XOR, and EQU (see Table I). These logic functions have been either described experimentally or suggested to occur on the basis of simulations using empirical data [49]. Actually, the prokaryotic transcription networks provide a large number of composite logic operators that are implemented through more complex natural or simulated regulatory setups. Alternatively, the CRM designs can be implemented by introducing mutations at the amino-acid sequences of the TFs and the base-pair (bp) sequences of the cis-regulatory regions [34]. Note that in our designs, the signaling molecules can serve as not only activators but also repressors by the introduction of an alternative promoter [50].

TABLE I. Logic operations for cis-regulatory input functions.

TFs		Logic functions					
S	X	AND	OR	ANDN	ORN	XOR	EQU
Low	Low	Off	Off	Off	On	Off	On
Low	High	Off	On	Off	Off	On	Off
High	Low	Off	On	On	On	On	Off
High	High	On	On	Off	On	Off	On
References		[3,33,37]	[33,37,47]	[34]	[48]	[33]	[33,34]

Then, we define the chemical species in Table II. All biochemical reactions are listed in Fig. 2(a), and some reaction constants are listed in Table III. Assume the fast reactions to be in equilibrium; refer to the equilibrium equations shown in Fig. 2(b), where square brackets stand for concentrations of species. In fact, the fast reaction equilibrium trick based on quasi-steady-state approximation approach has been widely applied to reduce the complexity of multiscale problems [18,54]. The conservation laws for DNA-binding sites in the regulatory regions are listed at the bottom of Fig. 2(c).

Define concentrations as our dynamical variables (see Table IV). Using equalities for the fast reactions and the conservation laws, we can eliminate fast variables. To that end, we can derive expressions of five CRIFs which are listed in Table V, and the rate equations which describe the evolutions of the concentrations of X, Y, L, and S monomers as follows:

TABLE II. Descriptions of species in biochemical reactions.

Species	Description
X	Protein CII
Y	Protein FtsH
L	Protein LuxI
S	Autoinducer AHL
C	LuxR-S complex
X_4	CII tetramer
C_2	Heterotetramer complex
P	RNA polymerase
D^X	DNA-binding site in cII gene
D^Y	DNA-binding site in ftsH gene
D^L	DNA-binding site in luxI gene
D_X^X	CII-DNA complex
D_C^X	LuxR-S-DNA complex
D_{CX}^X	CII-LuxR-S-DNA complex
D_{XC}^X	CII-LuxR-S-DNA complex

$$\frac{dX_i}{dt} = \mathrm{CRIF} - \delta_{xy} X_i Y_i - \delta_x X_i,$$

$$\frac{dY_i}{dt} = \alpha_y \frac{1+\mu_y X_i^4}{1+X_i^4} - \delta_y Y_i,$$

$$\frac{dL_i}{dt} = \alpha_l \frac{1+\mu_l X_i^4}{1+X_i^4} - \delta_l L_i,$$

$$\frac{dS_i}{dt} = \alpha_s L_i - \delta_s S_i + \eta(S_e - S_i), \tag{1}$$

where $S_e = \frac{Q}{N}\sum_{i=1}^{N} S_i$ (when N cells are considered), in which Q depends on the cell density in a nonlinear way. The rescaled parameters are also listed in Table IV.

B. Analysis

1. Phase-reduction approach

First, we rewrite the final equation in Eq. (1) as the following symmetric form of coupling:

$$\frac{dS_i}{dt} = \alpha_s L_i - \delta_s S_i - \eta(1-Q)S_i + \frac{1}{N}\sum_{j=1}^{N} \eta Q(S_j - S_i). \tag{2}$$

For convenience, the system composed of both the first three equations of Eq. (1) and the equation

$$\frac{dS_i}{dt} = \alpha_s L_i - \delta_s S_i - \eta(1-Q)S_i \tag{3}$$

is called as auxiliary system, which is assumed to generate a sustained oscillation. Then, we perform an analytical study of the entire system in the phase-model description, which holds in a weak-coupling case [55]. The main steps are as follows. For convenience, we express the system of globally coupled oscillators as

(a)

	Reaction	Scale
I	$4X \overset{K_1}{\rightleftharpoons} X_4$ $2C \overset{K_2}{\rightleftharpoons} C_2$ $S+\mathrm{LuxR} \overset{K_3}{\rightleftharpoons} C$ $D^X+X_4 \overset{K_4}{\rightleftharpoons} D_X^X$ $D^Y+X_4 \overset{K_5}{\rightleftharpoons} D_X^Y$ $D^L+X_4 \overset{K_6}{\rightleftharpoons} D_X^L$ $D^X+C_2 \overset{K_7}{\rightleftharpoons} D_C^X$	Fast
II	$D_X^X+C_2 \overset{K_8}{\rightleftharpoons} D_{XC}^X$ $D_C^X+X_4 \overset{K_9}{\rightleftharpoons} D_{CX}^X$	
III	$D^X+P \overset{K_{10}}{\rightarrow} D^X+P+n_X X$ $D^Y+P \overset{K_{11}}{\rightarrow} D^Y+P+n_Y Y$ $D^L+P \overset{K_{12}}{\rightarrow} D^L+P+n_L L$ $D_X^Y+P \overset{f_1 K_{11}}{\rightarrow} D_X^Y+P+n_Y Y$ $D_X^L+P \overset{f_1 K_{12}}{\rightarrow} D_X^L+P+n_L L$ $X+Y \overset{K_{13}}{\rightarrow} Y$ $L \overset{c}{\rightarrow} L+S$ $X \overset{d_1}{\rightarrow} \varnothing$ $Y \overset{d_2}{\rightarrow} \varnothing$ $L \overset{d_3}{\rightarrow} \varnothing$ $S \overset{d_4}{\rightarrow} \varnothing$	Slow
IV	$D_X^X+P \overset{f_1 K_{10}}{\rightarrow} D_X^X+P+n_X X$	
V	$D_C^X+P \overset{f_2 K_{10}}{\rightarrow} D_C^X+P+n_X X$	
VI	$D_{XC}^X+P \overset{f_1 f_2 K_{10}}{\rightarrow} D_{XC}^X+P+n_X X$ $D_{CX}^X+P \overset{f_1 f_2 K_{10}}{\rightarrow} D_{CX}^X+P+n_X X$	

(b)

Fast Reaction Equilibrium		
$[X_4]=K_1[X]^4$	$[C_2]=K_2[C]^2$	$[C]=K_3[S][\mathrm{LuxR}]$
$[D_X^X]=K_4[X_4][D^X]$	$[D_X^Y]=K_5[X_4][D^Y]$	$[D_X^L]=K_6[X_4][D^L]$
$[D_C^X]=K_7[C_2][D^X]$	$[D_{XC}^X]=K_8[C_2][D_X^X]$	$[D_{CX}^X]=K_9[X_4][D_C^X]$

(c)

Logic Function	Reaction	Conservation Law
AND	I-VI	(1)
OR	I, III-V	(2)
ANDN	I-IV	(1)
ORN	I, III, IV	(2)
XOR	I, III-V	(1)
EQU	I-III, VI	(1)
$[D^{XT}]=[D^X]+[D_X^X]+[D_C^X]+[D_{XC}^X]+[D_{CX}^X]$ $[D^{YT}]=[D^Y]+[D_X^Y]$ $[D^{LT}]=[D^L]+[D_X^L]$		(1)
$[D^{XT}]=[D^X]+[D_X^X]+[D_C^X]$ $[D^{YT}]=[D^Y]+[D_X^Y]$ $[D^{LT}]=[D^L]+[D_X^L]$		(2)

FIG. 2. (a) The biochemical reactions are classified as two classes: fast and slow; (b) the equilibrium equations for the fast reactions; (c) six logic operations and their biochemical reactions, where the corresponding conservation laws are listed at the bottom. The reaction rates used are experimentally reasonable; refer to [18].

$$\frac{dx_i}{dt} = f(x_i) + \frac{1}{N}\sum_{j=1}^{N} p(x_i, x_j), \quad 1 \le i \le N, \tag{4}$$

where $x_i=(X_i, Y_i, L_i, S_i)^T$; $f=(F_1, F_2, F_3, F_4)^T$, with $F_1=\mathrm{CRIF}-\delta_{xy}X_iY_i-\delta_x X_i$, $F_2=\alpha_y\frac{1+\mu_y X_i^4}{1+X_i^4}-\delta_y Y_i$, $F_3=\alpha_l\frac{1+\mu_l X_i^4}{1+X_i^4}-\delta_l L_i$, and $F_4=\alpha_s L_i-\delta_s S_i-\eta(1-Q)S_i$; and $p(x_i,x_j)=(0,0,0,\eta Q(S_j-S_i))^T$. Assume that the uncoupled oscillator has period T. By the theorem of Kuramoto [55], for a weakly perturbed system we can obtain the corresponding phase model:

$$\frac{d\phi_i}{dt} = 1 + \frac{1}{N} Z(\phi_i) \cdot \sum_{j=1}^{N} p(x_i(\phi_i), x_j(\phi_j)), \tag{5}$$

where each $x_i(\phi_i)$ is the point on the limit cycle having phase ϕ_i, the symbol "·" is the dot product of two vectors, and

TABLE III. Descriptions and values of raw parameters.

Description	Values	References
Dimerization equilibrium constant	$K_1=1.8\times10^{18}M^{-1}$, $K_2=K_3=2.5\times10^6M^{-1}$	[46,51]
Regulatory binding constant	$K_4=K_5=K_6=K_7=5\times10^6M^{-1}$	[46]
	$K_8=K_9=2.5\times10^6M^{-1}$	
Degradation rate of protein	$d_X=d_Y=\ln 2/10$ min^{-1}, $d_L=\ln 2/0.2$ min^{-1}	[52]
	$d_S=\ln 2/1.1$ min^{-1}	
Autoinducer synthesis rate	$c=1.1$ min^{-1}	[53]
Bulk rate of transcription and translation	$k_X=k_Y=k_L=k_C=30$ min^{-1}	[6,46]
Amplified factor of transcription rate	$f_X=f_Y=f_L=10$, $f_C=90$, $f_{XC}=f_{CX}=90$	[46]
Rate of repressor degradation by Y	$K_{XY}=2\times10^{-5}M^{-1}$	[18]
Plasmid copy number	$m_X=10$, $m_Y=1$, $m_L=50$	[46]
Concentration of LuxR	$[\mathrm{LuxR}]=1\times10^{-8}M^{-1}$	[18]
Other parameters	$n_XK_X[\mathrm{D^{XT}}][P]=8\times10^{-8}$ M min^{-1}, $n_X=n_Y=n_L=1$	[8]

$$Z(\phi_i) = \mathrm{grad}\ \phi_i(x_i). \tag{6}$$

$Z(\phi_i)$, a phase response function characterizing the phase advance per unit perturbation, is a 2π-period function with respect to ϕ_i. To study collective properties of the network, such as synchronization and clustering, it is convenient to represent each ϕ_i as $\phi_i=t+\vartheta_i$, with the first term capturing the fast free-running natural oscillation $d\phi_i/dt=1$, and the second term capturing the slow network-induced buildup of phase derivation from the natural oscillation. Substituting the expression of ϑ_i into Eq. (5) results in

$$\frac{d\vartheta_i}{dt} = \frac{1}{N}Z_i(t+\vartheta_i)\cdot\sum_{j=1}^{N}p(x_i(t+\vartheta_i),x_j(t+\vartheta_i)). \tag{7}$$

The classical method of averaging consists of a near-identity change of variables that transforms the system into the form

$$\frac{d\phi_i}{dt} = 1+\frac{1}{N}\sum_{j=1}^{N}H_{ij}(\phi_j-\phi_i), \tag{8}$$

where $H_{ij}(\Delta\phi)$ represents the interaction function with respect to the phase difference $\Delta\phi=\phi_j-\phi_i$ between two cells,

$$H_{ij}(\phi_j-\phi_i) = \frac{1}{T}\int_0^T Z_i(t)\cdot p(x_i(t),x_j(t+\phi_j-\phi_i))dt$$
$$= \frac{1}{2\pi}\int_0^{2\pi} Z_i(\theta)\cdot p(\phi_j-\phi_i+\theta)d\theta, \tag{9}$$

which can be calculated numerically [56]. In what follows, we omit subscripts i and j for convenience. From $H(\Delta\phi)$, we introduce a function, $G(\Delta\phi)=H(\Delta\phi)-H(-\Delta\phi)$, to determine the mode of coupling. If $G(\Delta\phi)$ exhibits a positive slope at $\Delta\phi=0$, i.e., $G'(0)>0$, the coupling is phase attractive. If $G'(0)<0$, the coupling is phase repulsive. Such an approach based on the sign of $G'(0)$ that depends generally on the intrinsic dynamics of the uncoupled oscillator and on the interaction between the oscillators is more effective than that of directly observing the network topology in determining the mode of weak coupling [23], especially in the case of complex network architectures.

According to Tables III and IV, we can estimate our system parameter values as follows: $\alpha_x=10$, $\alpha_y=1$, $\alpha_l=50$, $\alpha_s=0.4$, $\delta_x=0.5$, $\delta_y=0.5$, $\delta_l=25$, $\delta_s=45$, $\delta_{xy}=5$, $\mu_x=10$, $\mu_y=10$, $\mu_l=10$, $\mu_s=9$, $\mu_{xs}=90$, $\lambda=1$, $\eta=10$, and $Q=0.5$. For such a set of values, numerical simulation verifies that the term $\frac{1}{N}\Sigma_{j=1}^{N}\eta Q(S_j-S_i)$ affects the timing but not the amplitude of the auxiliary system for any $N\geq2$, so the above analysis is feasible. In addition, we emphasize that for other different experiments on multicellular systems with the quorum sensing [11–17], the differences between the rescaled

TABLE IV. Rescaled variables and rescaled parameters for models. We assume $K_2=K_3$, $K_4=K_5=K_6=K_7$, $K_8=K_9$, $K_X=K_Y=K_L=K_C$, $[\mathrm{D^{XT}}]=[\mathrm{D^{YT}}]=[\mathrm{D^{LT}}]=[\mathrm{D^{ST}}]$, and $n_X=n_Y=n_L=n_S=e$ for rescaling.

Rescaled variables	Rescaled parameters
$X=(K_4K_1)^{1/4}[\mathrm{X}]$	$\mu_x=f_X$, $\mu_y=f_Y$, $\mu_l=f_L$, $\mu_s=f_C$, $\mu_{xs}=f_{XC}K_8/K_7+f_{CX}K_9/K_4$
$Y=(K_4K_1)^{1/4}[\mathrm{Y}]$	$\alpha_x=m_X$, $\alpha_y=m_Yn_Y/n_X$, $\alpha_l=m_Ln_L/n_X$, $\tau^*=n_XK_X(K_1K_4)^{1/4}[\mathrm{D^{XT}}][\mathrm{P}]$
$L=(K_4K_1)^{1/4}[\mathrm{L}]$	$\alpha_s=cK_3(K_2K_7)^{1/2}[\mathrm{LuxR}]/[(K_1K_4)^{1/4}t^*]$, $t=\tau^*\tau$, $\delta_x=d_X/\tau^*$, $\delta_y=d_Y/\tau^*$
$S=K_3(K_2K_7)^{1/2}[\mathrm{LuxR}][\mathrm{S}]$	$\delta_l=d_L/\tau^*$, $\delta_{xy}=K_{XY}/[(K_1K_4)^{1/4}\tau^*]$, $\delta_s=d_S/\tau^*$, $\lambda=K_8/K_7+K_9/K_4$

TABLE V. Biochemical reactions and cis-regulatory input functions for relaxation oscillators.

Logic function	CRIF
AND	$\alpha_x \frac{1+\mu_x X^4+\mu_s S^2+\mu_{xs} X^4 S^2}{1+X^4+S^2+\lambda X^4 S^2}$
OR	$\alpha_x \frac{1+\mu_x X^4+\mu_s S^2}{1+X^4+S^2}$
ANDN	$\alpha_x \frac{1+\mu_x X^4}{1+X^4+S^2+\lambda X^4 S^2}$
ORN	$\alpha_x \frac{1+\mu_x X^4}{1+X^4+S^2}$
XOR	$\alpha_x \frac{1+\mu_x X^4+\mu_s S^2}{1+X^4+S^2+\lambda X^4 S^2}$
EQU	$\alpha_x \frac{1+\mu_{xs} X^4 S^2}{1+X^4+S^2+\lambda X^4 S^2}$

parameter values are not so large that they abolish our conclusions.

2. Determining the stability of balanced clustering

Balanced clusters mean that N oscillators are divided into M subgroups of equal cell number with each subgroup being synchronized and with the equal phase difference between neighboring subgroups. Here, we employ the approach of Okuda [57] to determine the stability of such clusters (see the Appendix of this paper for details). In that method, we need to calculate two kinds of eigenvalues: one is associated with intracluster fluctuations and the other with intercluster fluctuations, which are denoted by λ_p and λ_q, respectively, where $M \le p \le N-1$ and $0 \le q \le M-1$, with M being the number of clusters presumptively. For convenience, denote by $\lambda^{(1)}$ and $\lambda^{(2)}$ the $N-M$ same eigenvalues λ_p and the maximum of the real parts of $(M-1)$ nonzero eigenvalues λ_q, respectively. By calculation, we find $\lambda_p = 1/M \Sigma_{k=0}^{M-1} \Gamma'(2\pi k/M)$, with $p=M, M+1, \ldots, N-1$, and $\lambda_q = 1/M \Sigma_{k=0}^{M-1} \Gamma'(2\pi k/M)[1-\exp(-i2\pi kq/M)]$, with $q = 0, 1, \ldots, M-1$, where $\Gamma(\Delta\phi) = H(-\Delta\phi)$. Then, the stability of clusterings can be determined by the signs of $\lambda^{(1)}$ and $\lambda^{(2)}$. Specifically, the clustering is stable if both $\lambda^{(1)}$ and $\lambda^{(2)}$ are negative, and is unstable if $\lambda^{(2)}$ is positive. In addition, if $\lambda^{(1)}$ is positive and $\lambda^{(2)}$ is negative, and further if $M=N$, the M cluster (i.e., the splay state) is also stable.

In Secs. III and IV, we will numerically study cooperative behaviors of coupled genetic relaxation oscillators with different CRMs. In contrast to the previous works [18–29], we will show that different CRMs can drive fundamentally different dynamic patterns.

III. CASE OF TWO COUPLED CELLS: PHASE LOCKING

Synchronization and clustering of genetic oscillators coupled to quorum sensing result from the interplay between the intrinsic properties of the individual cells, the type of cellular communication, and the network topology. To gain insights into the rules governing dynamic patterns in complex networks of cells, here we investigate the case of two coupled genetic oscillators in detail.

First, based on Eq. (8) the phase model of two coupled oscillators can be characterized by

$$\frac{d\phi_1}{dt} = 1 + H(\Delta\phi),$$

$$\frac{d\phi_2}{dt} = 1 + H(-\Delta\phi), \tag{10}$$

where the phase difference is denoted as $\Delta\phi = \phi_2 - \phi_1$. The interplay between the two oscillators is often described by the evolution of the phase difference $\Delta\phi$, which is determined solely by the odd part of the effective coupling function $G(\Delta\phi)$, i.e., $H(\Delta\phi) - H(-\Delta\phi)$. That is, the dynamics of $\Delta\phi$ is given by

$$\frac{d\Delta\phi}{dt} = -G(\Delta\phi). \tag{11}$$

The zero points of $G(\Delta\phi)$ are the fixed points of Eq. (11). These fixed points describe the phase-locked states of two coupled cells and their stabilities are determined by the sign of slope of the curve $G(\Delta\phi)$ at the zero points. A positive slope means that the corresponding fixed point is stable, implying that $\Delta\phi$ near the fixed point dynamically converges to the fixed point, whereas a negative slope means that the fixed point is unstable, implying that $\Delta\phi$ close to the fixed point dynamically diverges. The size of the slope determines the convergence or divergence rate at the fixed point. The functions $G(\Delta\phi)$ corresponding to five logic operations AND, OR, ANDN, ORN, and XOR are shown in Figs. 3(a)–3(e), respectively (here and below we did not investigate the case of EQU due to the fact that the EQU destroys the dynamics of the core relaxation oscillator in the region of biological reasonable parameters, leading to the loss of sustained oscillation), whereas the interaction functions $H(\Delta\phi)$ are shown in the insets.

AND and OR. The function $G(\Delta\phi)$ in Figs. 3(a) and 3(b) equates to zero at $\Delta\phi=0$ with positive slope and at $\Delta\phi=\pi$ with negative slope. Moreover, the zero point $\Delta\phi=0$ is the unique stable state of Eq. (11). Therefore, the phase-model analysis predicts that the phase difference of any initial values except $\Delta\phi=\pi$ eventually converges to $\Delta\phi=0$. This result is also verified by integrating the original model with various initial values. A typical snapshot is plotted in the upper left of Fig. 3(f). Thus, the analysis together with numerical simulation shows that AND and OR play a role in stabilizing the in-phase synchronization for two coupled cells. In this case, the coupling is phase attractive.

ANDN and ORN. Equation (11) has one unstable state $\Delta\phi=0$ and one stable state $\Delta\phi=\pi$, both of which correspond to zero points of the function G, as shown in Figs. 3(c) and 3(d). The role of ANDN and ORN is to stabilize the antiphase state and prevent the in-phase state. More precisely, the integration between the intracellular activator and intercellular signaling repressor in our model destabilizes the in-phase synchronization. In this case, the coupling is phase repulsive. A typical snapshot is plotted in the upper right of Fig. 3(f).

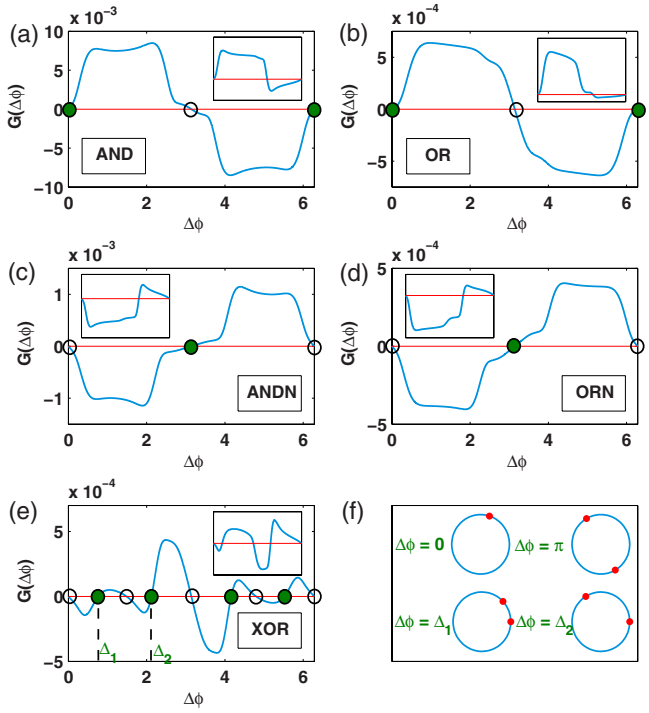

FIG. 3. (Color online) The dependence of the function G on phase difference $\Delta\phi$ in $[0,2\pi]$ and the distribution of its zero points in the case of two coupled oscillators. In (a)–(d), G has three zero points, two of which are unstable and the other one is unstable in the cases of AND and OR, whereas one is stable and the other two are unstable in the cases of ANDN and ORN. In (e), G corresponding to XOR has four stable zero points and five unstable zero points. In all the cases, filled circles represent stable points and open circles represent unstable points, and insets display the corresponding $H(\Delta\phi)$ of the auxiliary system. In (f), some typical instantaneous distributions of phases are demonstrated in the five cases of logic operations.

XOR. The function G has nine zero points, four of which, denoted by $\Delta\phi=\Delta_1,\Delta_2$ and $\Delta\phi=\pi+\Delta_1,\pi+\Delta_2$, respond to stable states of Eq. (11) and the other five to unstable states, as shown in Fig. 3(e). The unstable states form the boundaries for the attraction basins of the stable states. The role of XOR is to stabilize four out-of-phase states with phase differences $\Delta\phi=\Delta_1,\Delta_2$ and $\Delta\phi=\pi+\Delta_1,\pi+\Delta_2$, respectively, whereas it destabilizes the in-phase and antiphase states. Two typical snapshots are shown in the bottom row of Fig. 3(f).

IV. CASE OF A POPULATION OF CELLS: SYNCHRONIZATION AND CLUSTERING

In this section, we investigate the case of N coupled genetic oscillators ($N>2$), focusing on two dynamical behaviors, i.e., synchronization and clustering, which are ensemble phenomena observed commonly in natural and artificial populations of (possibly weakly) interacting oscillators. Synchronization is a cooperative in-phase behavior, which has been the subject of numerous studies in physics and biology [55,58–60], whereas clustering is a fragmentation of the collective behavior in locally synchronized but well-separated subgroups, which has been also observed in numerous contexts with distinct contributions [57,61–69]. In what follows, we investigate balanced clustering and nonbalanced clustering separately for clarity. (Note that synchronization is a particular type of clustering, i.e., one clustered.)

A. Balanced clustering

In the analysis part, we present an approach for determining the stability of balanced clustering. Here, we display numerical results for balanced clustering. In particular, we show that CRMs of the different structure play different roles in the achievement of collective behaviors.

AND. Figure 4(a) indicates that one- and three-cluster states are stable since both λ_1 and λ_2 are negative. The instantaneous phase distributions on the unit cycle as shown in Fig. 4(b) verify the coexistence of stable complete synchronization and three-cluster state.

OR. In this case, the eigenvalues shown in Fig. 4(c) indicate that only the complete synchronization (one clustered) is stable, which is verified by the numerical simulation shown in Fig. 4(d). The analysis together with the numerical simulation shows that the OR plays the role of stabilizing complete synchronization; i.e., for any initial conditions for these oscillators, the systems consequentially evolve into a stable complete synchronization.

ANDN. The stability analysis of the eigenvalues shown in Fig. 4(e) reveals that the network of coupled oscillators with the ANDN possesses complex cluster-balanced states, e.g., the stable three-, five-, and eight-cluster states. These clustering states are numerically implemented as shown in Fig. 4(f).

ORN. We give the results on the stability analysis as shown in Fig. 4(g), which indicate that the population of oscillators can give rise to more complex cluster-balanced states than those displayed in the case of ANDN. For example, two additional cluster-balanced states, 9- and 11-cluster states, are found. The instantaneous phase distributions of these clustering states on the unit cycle are shown in Fig. 4(h).

XOR. In this case, the system of coupled oscillators possess only a stable cluster-balanced state (three clustered) that can be seen from the sign of two eigenvalues determining the stability [see Fig. 4(i)]. A snapshot of the unique balanced clustering is shown in Fig. 4(j).

To display cellular patterns more clearly, we also plot all the time courses of the component X in the case of ORN; refer to Fig. 5. These cluster states appearing in the cases of different logic operations indicates that different CRMs can drive fundamentally different cellular patterns.

B. Nonbalanced clustering

Except for balanced clustering as shown in Sec. IV A, we also find nonbalanced clustering. However, finding all nonbalanced clusterings is much more difficult than finding all balanced clusterings since in the former, one needs to search for all stable regions of initial values of coupled systems that lead to stable nonbalanced clusterings, and this is even impossible only with computer simulation when the cell

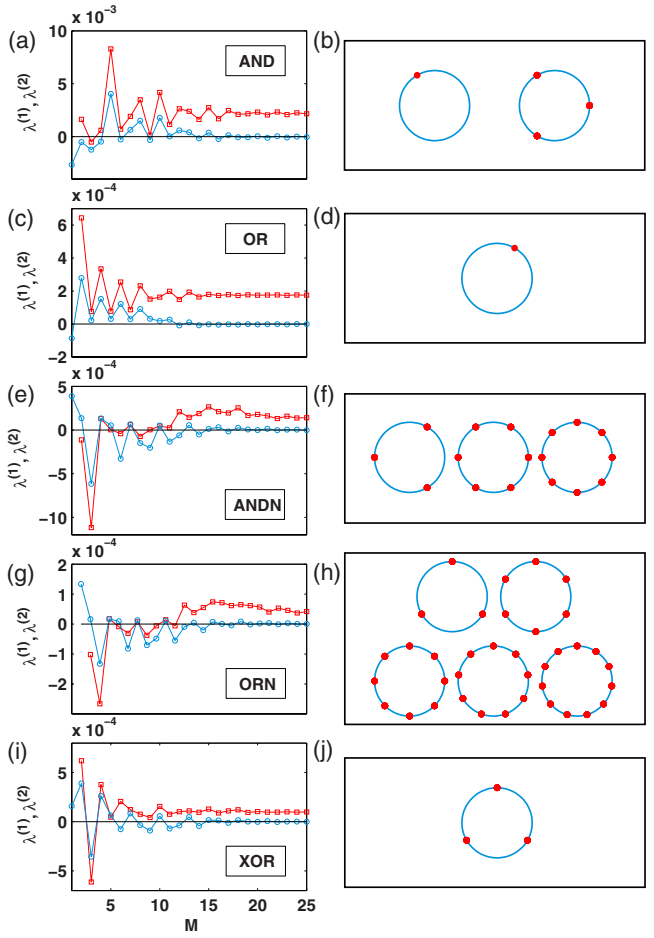

FIG. 4. (Color online) Left panel: eigenvalues associated with intracluster fluctuations λ_1 (blue cycle) and the maximal real part of nonzero eigenvalues associated with intercluster fluctuations λ_2 (red square) as a function of the number of balanced clusters with five different logic functions. Right panel: the corresponding instantaneous phase distribution of all possible balanced clusters for [(a) and (b)] 1- and 3-cluster states for AND; [(c) and (d)] 1-cluster state (complete synchronization) for OR; [(e) and (f)] 3-, 6-, and 8-cluster states for ANDN; [(h) and (i)] 3-, 6-, 8-, 9-, and 11-cluster states for ORN; and [(j) and (k)] 3-cluster state for XOR. Different clustering states appear due to different choices of initial conditions but the cell number is fixed as $N=792$.

number is large. Here, we mainly want to show that nonbalanced clusterings are existent in some cases of five logic operations. By numerical simulation, we find that different CRMs can drive different types of nonbalanced clusterings except for the OR case (since the complete synchronization is globally stable). Taking the cases of ORN and XOR as examples, we find several typical nonbalanced clusterings which are displayed in Fig. 6. In the case of ORN, we find five- and six-cluster states, whereas in the case of XOR, we find a four-cluster state and two different types of five-cluster states. Note that we did not search out all nonbalanced clusterings, and other types of nonbalanced clusterings except for those found are possible, but would depend on the number of oscillators and the choice of initial conditions.

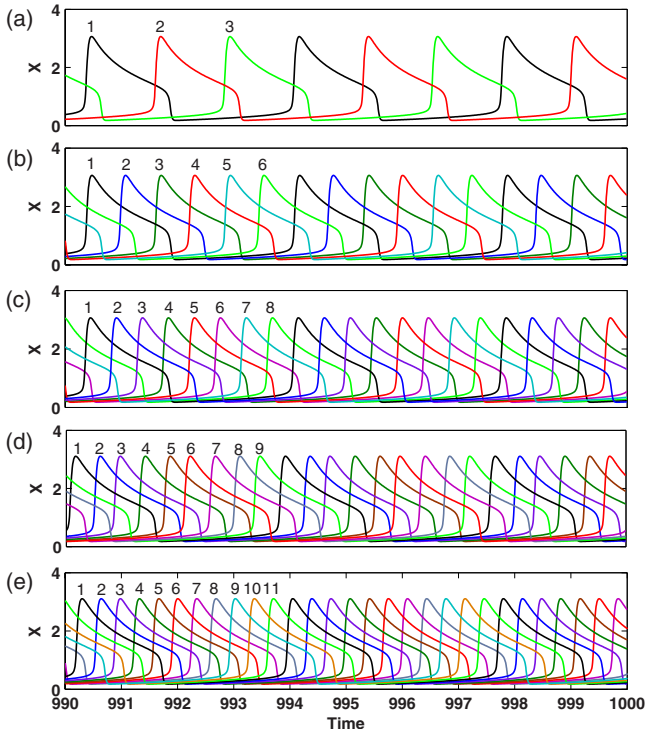

FIG. 5. (Color online) Temporal evolutions of the concentration of X corresponding to ORN in Fig. 4: (a) 3-cluster state, (b) 6-cluster state, (c) 8-cluster state, (d) 9-cluster state, and (e) 11-cluster state, where each cluster state is indicated by different color or an integer. For each obtained cluster state, numerical integration begins from an initial condition close to the corresponding clustering, and plot shown begins after allowing a transient time of 10^4 units.

V. EFFECT OF REWIRING NETWORK ON SYNCHRONIZATION AND CLUSTERING

Biological rhythm results from the interplay between the intrinsic properties of the individual cells, the properties of the communication, as well as the network topology. Each property may play an important role in shaping the emergent synchronous behavior. Except that different CRMs can drive different cellular patterns shown in Secs. III and IV, the rewiring architecture of individual cells also may play a significant role in promoting synchronization or antisynchronization of coupled cells. For example, it has been shown that rewired interaction in a repressilator population with cell-to-cell communication can offer diverse dynamics, such as multistability and clustering [23,28]. Note that in the above investigated models, the signal molecule regulates an activator, thus performing an activator-regulated communication. Due to biological background of the core genetic oscillator and the quorum sensing, however, the signal molecule can also regulate a repressor, leading to so-called repressor-regulated communication in contrast to activator-regulated communication. In this section, we investigate the effect of this rewiring architecture of motifs on synchronization and clustering.

In contrast to the scheme of signal integration in Secs. III and IV [refer to the simplified scheme shown in Fig. 7(a)], in what follows we rewire the interaction of the signaling molecule and its regulated gene inside the cell [16,27], as shown

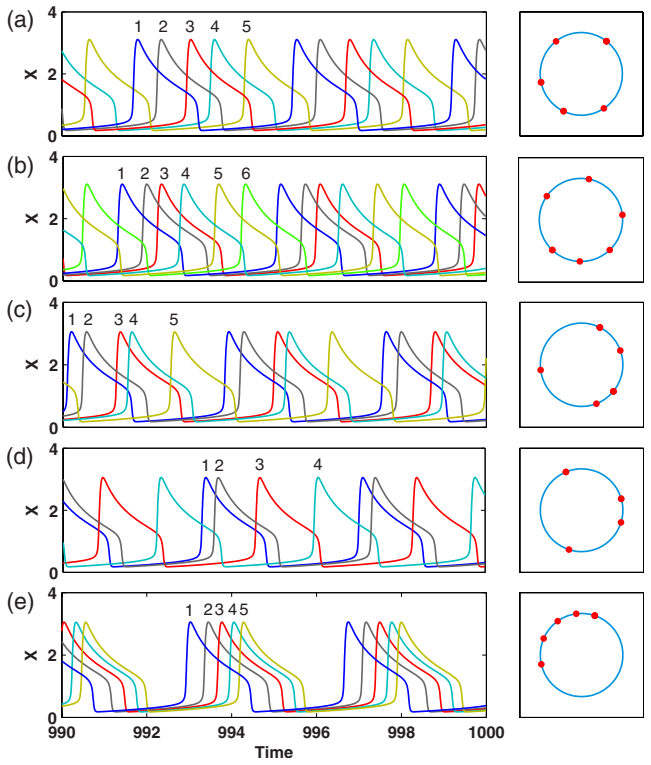

FIG. 6. (Color online) Nonbalanced clusterings found in the cases of ORN and XOR. Left panel: temporal evolutions of the concentration of X corresponding to ORN and XOR. Right panel: cellular patterns for (a) five-cluster state for ORN; (b) six-cluster state for ORN; (c) five-cluster state for XOR; (d) four-cluster state for XOR; and (e) five-cluster state for XOR, where each cluster state is indicated by different color or an integer. For each shown nonbalanced clustering, numerical integration begins from an initial condition close to the corresponding clustering, and plot shown begins after allowing a transient time of 10^4 units.

in Fig. 7(b). More precisely, we let the signaling molecule AI and the TF X combinatorially regulate the target gene y instead of gene x. Completely similarly, we can derive expressions of six possible CRIFs (see Table V), and the dynamical equations describing the time evolution of the concentrations of X, Y, L, and S monomers in the following forms:

$$\frac{dX_i}{dt} = \alpha_x \frac{1+\mu_x X_i^4}{1+X_i^4} - \delta_{xy} X_i Y_i - \delta_x X_i,$$

$$\frac{dY_i}{dt} = \mathrm{CRIF} - \delta_y Y_i,$$

$$\frac{dL_i}{dt} = \alpha_l \frac{1+\mu_l X_i^4}{1+X_i^4} - \delta_l L_i,$$

$$\frac{dS_i}{dt} = \alpha_s L_i - \delta_s S_i + \eta(S_e - S_i), \tag{12}$$

where the CRIFs are similar to those in the case of activator-regulated communication (refer to Table V) except that parameters α_x and μ_{xs} are replaced by α_y and μ_{ys}, respectively.

Architecture	(a)	(b)
AND	1, 3	1, 2, 4, 5
OR	1	1, 2, 3
ANDN	3, 6, 8	5, 8
ORN	3, 6, 8, 9, 11	5, 8
XOR	3	5, 8

FIG. 7. (Color online) Different balanced clusterings of original and rewired genetic architectures: (a) activator-regulated communication and (b) repressor-regulated communication. The corresponding clusterings for two cases are listed at the bottom, respectively. Note: only the same balanced clusterings are shown for three logic operations in the case of repressor-regulated communication, but different nonbalanced clusterings are possible (data are not shown here).

In both cases, the settings of parameter values are also the same except for $\mu_{ys}=90$. The numerical results are summarized in Fig. 7, where all balanced clusterings are listed in two cases of activator-regulated communication and repressor-regulated communication for comparison. From Fig. 7, we see that different CRMs also can drive fundamentally different cellular patterns in the case of repressor-regulated communication, but the wave patterns are different from those in the case of activator-regulated communication (data for comparison are not shown). In addition, we show how the odd part of the interaction function $H(\Delta\phi)$, $G(\Delta\phi)$, in the five logic operations, changes with phase difference $\Delta\phi \in [0, 2\pi]$ in Fig. 8, where stable zero points (symbolized as filled circles) and unstable zero points (symbolized as open circles) are shown. Our results suggest that the architecture of biological systems might make them particularly evolvable, namely, simple shuffling of finely tuned network architectures may render new functionalities of networks with feedforward and feedback.

The rational design of biological networks and pathways promises to reveal ways of rewiring cells for new biological functions or of gaining insights into the behavior of natural systems. Much of the work to date has focused on the manipulation of transcriptional and post-transcriptional elements to create synthetic gene networks with desired functions [4,6,70–72]. In contrast, our present study provides a possible arsenal for designing and constructing a network of genetic oscillators with a different cellular behavior, indicating that rationally reprogramming integration of two input TFs by changing a CRM to activate a targeted gene could be used to induce transition among various cellular patterns toward the corresponding desired functions. In spite of this, we expect that understanding how different CRMs render different responses for the coupled genetic oscillators with quorum sensing would provide a valuable insight into designing new synthetic genetic circuits.

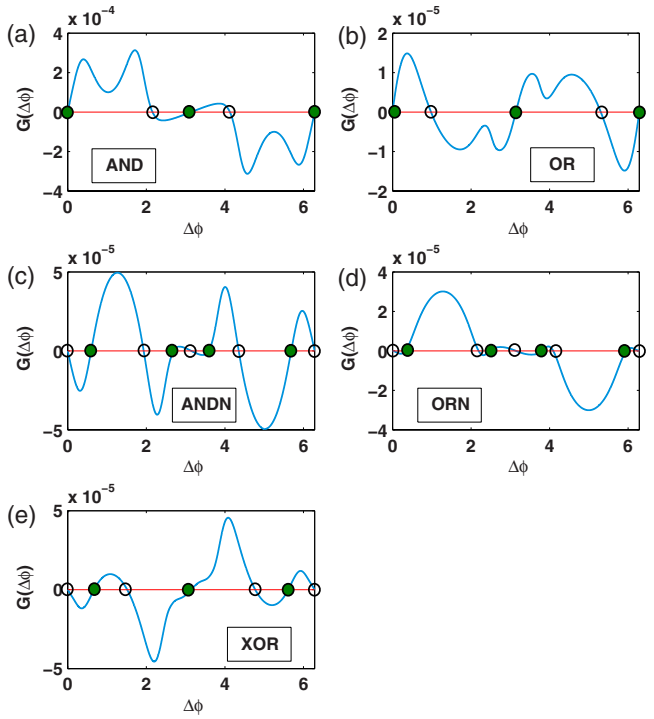

FIG. 8. (Color online) The dependence of the function $G(\Delta\phi)$ on phase difference $\Delta\phi$, where its stable zero points (filled circles) and unstable zero points (open circles) are shown.

VI. CONCLUSION AND DISCUSSION

Using models of synthetic genetic relaxation oscillators coupled with quorum sensing, we have shown both analytically and numerically that different CRMs drive fundamentally different cellular patterns, such as synchronization and balanced clustering, and nonbalanced clustering, by considering two types of communications: activator-regulated communication and repressor-regulated communication. Specifically, in the case of two coupled oscillators, we have shown that different CRMs have marked influences on characteristics of phase-locking processes. For example, two oscillators can display in-phase, antiphase, and out-of-phase synchronization with a certain constant phase difference, depending on the type of CRM. In the case of $N(>2)$ coupled oscillators with activator-regulated communication, there are 1 and 3 balanced clusters for AND; only 1 balanced cluster for OR; 3, 6, and 8 balanced clusters for ANDN; 3, 6, 8, 9, and 11 balanced clusters for ORN; and only 3 balanced clusters for XOR. On the other hand in the case of N coupled cells with repressor-regulated communication, there are 1, 2, 4, and 5 balanced clusters for AND; 1, 2, and 3 balanced clusters for OR; 5 and 8 balanced clusters for ANDN, ORN, and XOR. In addition, some nonbalanced clusters have been also found. These results would provide a strategy for a network of genetic oscillators: the selection of cooperative rhythmic manner, e.g., synchronization and clustering, is governed by the nature of the integration of the intracellular signal and the secretion of the biochemical signals through which the oscillating cells are globally coupled. In particular, genetic network architecture found in synchronous circadian clocks [73] might be constrained since the complete synchronization independent of initial conditions takes place only in the case of OR type of response. In addition, our results would imply that multicellular organisms evolve into some functional CRMs for particular goals (e.g., cellular patterns) by performing an elaborate computation for input TFs.

We expect that our findings will stimulate further investigations under a more realistic condition involving stochasticity [21,74–76] and heterogeneity [19] as specified in the following four points:

(1) In a stochastic environment, we should consider the stability of the obtained desired dynamic pattern. Theoretically, Golomb *et al.* [61] showed that the clustering state is stable on the condition that noise intensity is below a critical value. On the other hand, the global noise can enhance the extent of phase synchronization [77], but also can destroy the clustering state like in slow switching [78]. Therefore, we should carefully design the CRM structure in the presence of noise to preserve the desired dynamic patterns.

(2) In our model, a population of identical oscillators communicate with a uniform coupling, but it would be of great interest to study the influence of the cellular variability and coupling strength heterogeneity on the synchronization and clustering. If heterogeneity is sufficiently small compared to the coupling strength, we can treat the system as that of identical oscillators. Otherwise, the effect of heterogeneity should be considered. In fact, it has been shown that heterogeneous coupling strength and element variability can make the occurrence of clustering states possible in networks of neural oscillators [79]. Similarly, in our case, heterogeneity would result in synchronization and clustering.

(3) Our results were obtained under the condition that the intercellular communication is rather weak. However, it is likely that coupling is stronger than that considered here [23,80]. Therefore, it would be of interest to analyze dynamical patterns in the case of strong coupling. In this case, other modes of complex behaviors such as multistability [23,24], inhomogeneous limit cycle [23,29], oscillation death [20,23], aperiodic oscillation [81], and chaos [29,81] may also appear in our models.

(4) We point out that our results are in general robust against changes in parameter values if they are not chosen close to the margin of oscillation of the uncoupled oscillator. For a kind of response (e.g., the response of AND type), however, modes of clustering possibly depend on parameter values. For example, for a set of parameter values given above, two kinds of clustering modes in the case of AND have been found and displayed, but for a different set of parameter values, other kinds of clustering modes are possible. In addition, in the case that parameter values are chosen close to the margin of oscillation of the uncoupled oscillator, the system can display richer dynamical behaviors expected to be further investigated, but the phase-reduction approach of Kuramoto [61] cannot be used.

In addition, we point out that many theoretical studies have shown that biological oscillators intertwined with positive and negative feedback loops should have the following essential requirements [82,83]. First, negative feedback is necessary to carry a reaction network back to the "starting point" of its oscillation. Second, the negative feedback signal

must be sufficiently delayed in time so that the chemical reactions do not settle on a stable steady state. Third, the kinetic rate laws of the reaction mechanism must be sufficiently "nonlinear" to destabilize the steady state. Fourth, the reactions that produce and consume the interacting chemical species must occur on appropriate time scales that permit the network to generate oscillations. Facing to the complexity of gene regulatory networks, these mathematical insights reveal the true nature of gene relaxation oscillators. Our core relaxation oscillator can show sustained and robust oscillation under the guarantee of the above theoretical results. Especially, our coupled positive and negative feedback biological oscillator models rely on a separation of time scales between the two components to create relaxation oscillations; i.e., the activator must have faster dynamics than that of the repressor. To that end, we can increase the plasmid copy number concentrations as well as degradation rates of activator, where high degradation rate has artificially been implemented by using peptide sequences appended to the protein to make it a target for proteases in the cell [6,84]. Therefore, it would be possible to experimentally demonstrate our circuit design. It would be much more useful to take a hybrid approach in which experiments and modeling can be performed in parallel to advance one another. In a cyclic fashion, experiments can be used to inform the designs of mathematical models, which can in turn be used to make experimentally testable predictions.

Finally, ongoing structural, biochemical, and cell-based studies have begun to reveal several common principles by which protein components are used to specifically transmit and process information. Our studies demonstrate that these relatively simple principles can be used to rewire signaling behaviors in a process that mimics the evolution of new phenotypic responses. We expect that our work would motivate the investigations in areas such as development, where epigenetic inheritance leads to a persistent phenotypic alteration in response to transient signals, or in cell-to-cell communication systems that coordinate the rich complexity of group behaviors.

ACKNOWLEDGMENTS

This work was supported by the Natural Science Key Foundation of People's Republic of China (Grant No. 60736028).

APPENDIX: OKUDA'S APPROACH

In this appendix, we define cluster-balanced states and study their stability. Each cluster contains the same number of oscillators. Thus, we restrict our attention mainly on symmetric states.

Assume that the phase model of N oscillators is governed by

$$\frac{d\phi_i}{dt} = \Omega + \frac{1}{N}\sum_{j=1}^{N} \Gamma(\phi_i - \phi_j), \tag{A1}$$

where $i=1,2,\ldots,N$. Although Ω can be given any value in a suitable moving coordinate, we assume $\Omega=0$ below without explicitly referring to it. First, we define a symmetric M-cluster state as the state in which N/M oscillators belong to each of M clusters. Since no randomness is included in the system, all the oscillators in a certain cluster should be located at the same phase. Let Φ_k denote the phase of cluster k $(k=0,1,\ldots,M-1)$. From the phase equation, we obtain the equation for Φ_k as

$$\Phi_k = \frac{1}{M}\sum_{l=0}^{M-1} \Gamma(\Phi_k - \Phi_l). \tag{A2}$$

We seek solutions to this equation in the form

$$\Phi_k = \omega^{(M)} t + \frac{2\pi k}{M}, \tag{A3}$$

which implies that the phases of the M clusters are equally separated and rotate at a constant frequency $\omega^{(M)}$. Substituting it into the above phase equation, we find that the solution of the above form exists if

$$\omega^{(M)} = \frac{1}{M}\sum_{k=0}^{M-1} \Gamma\left(\frac{2\pi k}{M}\right). \tag{A4}$$

Next, we analyze the stability of the balanced M-cluster state. Let us set $\delta\phi_i = \phi_i - \Phi_k$ (where i belongs to cluster k) and express the linearized equation for $\delta\phi_i$ as $d\delta\Phi = J\Phi$, where the vector notation $\delta\Phi = (\delta\phi_1, \delta\phi_2, \ldots, \delta\phi_N)$ and $N\times N$ matrix J have been used. Without loss of generality, we assume that cluster k consists of the oscillators with $kN/M < i \le (k+1)N/M$. Then, we have

$$J = \begin{pmatrix} \alpha I - \beta_0 E & -\beta_1 E & \cdots & -\beta_{M-1} E \\ -\beta_{M-1} E & \alpha I - \beta_0 E & \cdots & -\beta_{M-2} E \\ \cdots & \cdots & \cdots & \cdots \\ -\beta_1 E & -\beta_2 E & \cdots & \alpha I - \beta_0 E \end{pmatrix}, \tag{A5}$$

where I is the $N/M \times N/M$ unit matrix and E is a matrix of the same dimension whose components are all 1, α and β_k are expressed as

$$\alpha = \frac{1}{M}\sum_{k=0}^{M-1} \Gamma'\left(\frac{2\pi k}{M}\right), \quad \beta_k = \frac{1}{N}\Gamma'\left(-\frac{2\pi k}{M}\right), \tag{A6}$$

and primes indicate the derivative with respect to the argument. Since J is a cyclic matrix, the explicit form of the characteristic equation of J can be obtained as

$$\begin{aligned} |\lambda I - J| &= \prod_{q=0}^{M-1} \left| (\lambda - \alpha) I + \left(\sum_{k=0}^{M-1} \beta_k e^{i2\pi kq/M} E \right) \right| \\ &= (\lambda - \alpha)^{N-M} \prod_{q=0}^{M-1} \left(\lambda - \alpha + \frac{N}{M} \sum_{k=0}^{M-1} \beta_k e^{i2\pi kq/M} \right) = 0, \end{aligned} \tag{A7}$$

where $i = \sqrt{-1}$. In this way, we obtain N eigenvalues of J in

the forms

$$\lambda_p \equiv \alpha = \frac{1}{M}\sum_{k=0}^{M-1} \Gamma'\left(\frac{2\pi k}{M}\right), \quad p = M, M+1, N-1, \tag{A8}$$

$$\lambda_q \equiv \alpha - \frac{N}{M}\sum_{k=0}^{M-1} \beta_k e^{i2\pi kq/M} = \frac{1}{M}\sum_{k=0}^{M-1} \Gamma'\left(\frac{2\pi k}{M}\right)(1 - e^{-i2\pi kq/M}), \quad q = 0, 1, \ldots, M-1. \tag{A9}$$

[1] D. Bray, Nature (London) **376**, 307 (1995).
[2] R. Weiss, S. Basu, S. Hooshangi, A. Kalmbach, D. Karig, R. Mehreja, and L. Netravali, Nat. Comput. **2**, 47 (2003).
[3] J. C. Anderson, C. A. Voigt, and A. P. Arkin, Mol. Syst. Biol. **3**, 133 (2007).
[4] T. S. Gardner, C. R. Cantor, and J. J. Collins, Nature (London) **403**, 339 (2000).
[5] J. Kim, K. S. White, and E. Winfree, Mol. Syst. Biol. **2**, 68 (2006).
[6] M. B. Elowitz and S. Leibler, Nature (London) **403**, 335 (2000).
[7] M. R. Atkinson, M. A. Savageau, J. T. Myers, and A. J. Ninfa, Cell **113**, 597 (2003).
[8] J. Hasty, F. Isaacs, M. Dolnik, D. McMillen, and J. J. Collins, Chaos **11**, 207 (2001).
[9] J. Hasty, D. McMillen, and J. J. Collins, Nature (London) **420**, 224 (2002).
[10] D. Sprinzak and M. B. Elowitz, Nature (London) **438**, 443 (2005).
[11] L. C. You, R. S. Cox III, R. Weiss, and F. H. Arnold, Nature (London) **428**, 868 (2004).
[12] F. K. Balagadde, L. C. You, C. L. Hansen, F. H. Arnolod, and S. R. Quake, Science **309**, 137 (2005).
[13] K. Brenner, D. K. Karlg, R. Weiss, and F. H. Arnold, Proc. Natl. Acad. Sci. U.S.A. **104**, 17300 (2007).
[14] S. Basu, R. Mehreja, S. Thiberge, M. T. Chen, and R. Weiss, Proc. Natl. Acad. Sci. U.S.A. **101**, 6355 (2004).
[15] S. Basu *et al.*, Nature (London) **434**, 1130 (2005).
[16] E. L. Haseltine and F. H. Arnold, Appl. Environ. Microbiol. **74**, 437 (2008).
[17] F. K. Balagadde *et al.*, Mol. Syst. Biol. **4**, 187 (2008).
[18] D. McMillen, N. Kopell, J. Hasty, and J. J. Collins, Proc. Natl. Acad. Sci. U.S.A. **99**, 679 (2002).
[19] J. García-Ojalvo, M. B. Elowitz, and S. H. Strogatz, Proc. Natl. Acad. Sci. U.S.A. **101**, 10955 (2004).
[20] A. Kuznetsov, M. Kaern, and N. Kopell, SIAM J. Appl. Math. **65**, 392 (2004).
[21] T. S. Zhou, L. N. Chen, and K. Aihara, Phys. Rev. Lett. **95**, 178103 (2005).
[22] T. S. Zhou, J. J. Zhang, Z. J. Yuan, and A. L. Xu, PLoS One **2**, e231 (2007).
[23] E. Ullner, A. Zaikin, E. I. Volkov, and J. García-Ojalvo, Phys. Rev. Lett. **99**, 148103 (2007).
[24] A. Koseska, E. Volkov, A. Zaikin, and J. Kurths, Phys. Rev. E **75**, 031916 (2007).
[25] A. Koseska, A. Zaikin, J. García-Ojalvo, and J. Kurths, Phys. Rev. E **75**, 031917 (2007).
[26] A. Koseska, E. Volkov, A. Zaikin, and J. Kurths, Phys. Rev. E **76**, 020901(R) (2007).
[27] Z. J. Yuan, J. J. Zhang, and T. S. Zhou, Phys. Rev. E **78**, 031901 (2008).
[28] T. S. Zhou, J. J. Zhang, Z. J. Yuan, and L. N. Chen, Chaos **18**, 037126 (2008).
[29] E. Ullner, A. Koseska, J. Kurths, E. Volkov, H. Kantz, and J. García-Ojalvo, Phys. Rev. E **78**, 031904 (2008).
[30] C. Fuqua, S. C. Winans, and E. P. Greenberg, Annu. Rev. Microbiol. **50**, 727 (1996).
[31] J. Smith, C. Theodoris, and E. H. Davidson, Science **318**, 794 (2007).
[32] U. Alon, *An Introduction to Systems Biology: Design Principles of Biological Circuits* (Chapman and Hall, London/CRC, Cleveland, 2006).
[33] N. E. Buchler, U. Gerland, and T. Hwa, Proc. Natl. Acad. Sci. U.S.A. **100**, 5136 (2003).
[34] R. Hermsen, S. Tans, and P. R. ten Wolde, PLoS Comput. Biol. **2**, e164 (2006).
[35] S. Mangan and U. Alon, Proc. Natl. Acad. Sci. U.S.A. **100**, 11980 (2003).
[36] Y. Setty, A. E. Mayo, M. G. Surette, and U. Alon, Proc. Natl. Acad. Sci. U.S.A. **100**, 7702 (2003).
[37] A. E. Mayo, Y. Setty, S. Shavit, A. Zaslaver, and U. Alon, PLoS Biol. **4**, e45 (2006).
[38] A. W. Gregory, Nat. Rev. Genet. **8**, 206 (2007).
[39] Y. C. Tsai, Y. S. Choi, W. Ma, J. R. Pomerening, C. Tang, and J. E. Ferrell, Science **321**, 126 (2008).
[40] C. Liu, D. Weaver, S. Strogatz, and S. Reppert, Cell **91**, 855 (1997).
[41] I. Mihalcescu, W. H. Hsing, and S. Leibler, Nature (London) **430**, 81 (2004).
[42] J. R. Pomerening, S. Y. Kim, and J. E. Ferrell, Cell **122**, 565 (2005).
[43] M. J. Rust, J. S. Markson, W. S. Lane, D. S. Fisher, and E. K. O'Shea, Science **318**, 809 (2007).
[44] S. Yamaguchi, H. Isejima, T. Matsuo, R. Okura, K. Yagita, M. Kobayashi, and H. Okamura, Science **302**, 1408 (2003).
[45] J. Stricker, S. Cookson, M. R. Bennett, W. H. Mather, L. S. Tsimring, and J. Hasty, Nature (London) **456**, 516 (2008).
[46] M. Ptashne and A. Gann, *Genes & Signals* (Cold Spring Harbor Laboratory, Cold Spring Harbor, NY, 2002).
[47] S. Fernandez, V. Shingler, and V. De Lorenzo, J. Bacteriol. **176**, 5052 (1994).
[48] I. Erill, S. Campoy, and J. Barbe, FEMS Microbiol. Rev. **31**, 637 (2007).
[49] R. Silva-Rocha and V. de Lorenzo, FEBS Lett. **582**, 1237 (2008).
[50] K. A. Egland and E. P. Greenberg, J. Bacteriol. **183**, 382

(2001).
[51] Y.-S. Ho, M. Lewis, and M. Rosenberg, J. Biol. Chem. **257**, 9128 (1982).
[52] The protein degradation rate can be experimentally altered by augmenting or tagging the protein with addition amino.
[53] M. I. Moré, L. D. Finger, J. L. Stryker, C. Fuqua, A. Eberhard, and S. C. Winans, Science **272**, 1655 (1996).
[54] L. A. Segel, Bull. Math. Biol. **50**, 579 (1988).
[55] Y. Kuramoto, *Chemical Oscillations, Waves and Turbulence* (Springer-Verlag, Berlin, 1984).
[56] G. B. Ermentrout and N. Kopell, J. Math. Biol. **29**, 195 (1991).
[57] K. Okuda, Physica D **63**, 424 (1993).
[58] A. Pikovsky, M. Rosenblum, and J. Kurths, *Synchronization—A Universal Concept in Nonlinear Science* (Cambridge University Press, Cambridge, England, 2001).
[59] S. H. Strogatz, *Sync: The Emerging Science of Spontaneous Order* (Hyperion, New York, 2003).
[60] S. Manrubia, A. S. Mikhailov, and D. H. Zanette, *Emergence of Dynamical Order* (World Scientific, Singapore, 2004).
[61] D. Golomb, D. Hansel, B. Shraiman, and H. Sompolinsky, Phys. Rev. A **45**, 3516 (1992).
[62] I. Z. Kiss, Y. Zhai, and J. L. Hudson, Phys. Rev. Lett. **94**, 248301 (2005).
[63] I. Z. Kiss, C. G. Rusin, H. Kori, and J. L. Hudson, Science **316**, 1886 (2007).
[64] A. F. Taylor, P. Kapetanopoulos, B. J. Whitaker, R. Toth, L. Bull, and M. R. Tinsley, Phys. Rev. Lett. **100**, 214101 (2008).
[65] C. W. Reynolds, Comput. Graph. **21**, 25 (1987).
[66] A. Y. Pogromsky, G. Santoboni, and H. Nijmeijer, Physica D **172**, 65 (2002).
[67] I. V. Belykh, V. N. Belykh, K. V. Nevidin, and M. Hasler, Chaos **13**, 165 (2003).
[68] M. Golubitsky, I. Stewart, and A. Torok, SIAM J. Appl. Dyn. Syst. **4**, 78 (2005).
[69] M. Golubitsky and I. Stewart, Bull., New Ser., Am. Math. Soc. **43**, 305 (2006).
[70] T. S. Bayer and C. D. Smolke, Nat. Biotechnol. **23**, 337 (2005).
[71] A. Becskei and L. Serrano, Nature (London) **405**, 590 (2000).
[72] R. Guantes and J. F. Poyatos, PLoS Comput. Biol. **2**, e30 (2006).
[73] J. C. Dunlap and J. J. Loros, Cell **96**, 271 (1999).
[74] J. M. Raser and E. K. O'Shea, Science **309**, 2010 (2005).
[75] N. Barkai and S. Leibler, Nature (London) **403**, 267 (2000).
[76] J. J. Zhang, Z. J. Yuan, J. W. Wang, and T. S. Zhou, Phys. Rev. E **77**, 021101 (2008).
[77] Y. Kawamura, H. Nakao, K. Arai, H. Kori, and Y. Kuramoto, Phys. Rev. Lett. **101**, 024101 (2008).
[78] H. Kori and Y. Kuramoto, Phys. Rev. E **63**, 046214 (2001).
[79] Y. X. Li, Y. Q. Wang, and R. Miura, J. Comput. Neurosci. **14**, 139 (2003).
[80] D. Golomb and J. Rinzel, Physica D **72**, 259 (1994).
[81] D. Gonze, N. Markadieu, and A. Goldbeter, Chaos **18**, 037127 (2008).
[82] J. J. Tyson and H. G. Othmer, Prog. Theor. Biol. **5**, 1 (1978).
[83] B. Novak and J. J. Tyson, Nat. Rev. Mol. Cell Biol. **9**, 981 (2008).
[84] S. Gottesman, E. Roche, Y. Zhou, and R. T. Sauer, Genes Dev. **12**, 1338 (1998).